IEEE Open Journal of
Power Electronics

Received 27 May 2022; accepted 10 June 2022. Date of publication 16 June 2022;
date of current version 28 June 2022. The review of this article was arranged by Associate Editor Liangzong He.

Digital Object Identifier 10.1109/OJPEL.2022.3183600

Geometry-Based Circuit Modeling of Quasi-Static Cavity Resonators for Wireless Power Transfer

TAKUYA SASATANI [1] (Member, IEEE), MATTHEW CHABALKO[2], YOSHIHIRO KAWAHARA [1] (Member, IEEE), AND ALANSON SAMPLE [3] (Member, IEEE)

[1]The University of Tokyo, Bunkyo-ku 113-8656, Japan
[2]Disney Research, Pittsburgh, PA 15213 USA
[3]University of Michigan, Ann Arbor, MI 48109 USA

CORRESPONDING AUTHOR: TAKUYA SASATANI (e-mail: sasatani@akg.t.u-tokyo.ac.jp)

This work was partially supported by JST ACT-X Grant JPMJAX190F, JST ERATO Grant JPMJER1501, and Value Exchange Engineering, a joint research project between Mercari, Inc. and the RIISE.

ABSTRACT Wireless power transfer technology has seen steady advances in recent years, yet seamlessly charging devices within large volumes of space remains challenging. Although quasi-static cavity resonators have recently demonstrated safe wireless power transfer at room-scale sizes at significant power levels, previous work investigated this concept using coupled mode theory, lacking utility from the engineering perspective. This work presents a circuit model analysis of quasi-static cavity resonance-based wireless power transfer systems, which creates a critical conceptual bridge to the electrical engineering community and reveals factors that dominate the system performance and power transfer efficiency. A closed-form circuit model is derived from the geometrical properties of the system by analyzing the field distribution of a cylindrical cavity structure and is experimentally validated using a room-scale quasi-static cavity resonator. Finally, we demonstrate the utility of the derived circuit model through case studies for designing impedance matching circuits and optimization of the QSCR geometry.

INDEX TERMS Circuit modeling, quasi-static cavity resonators, wireless power transfer.

I. INTRODUCTION

Wireless power transfer (WPT) systems promise to eliminate the need for wired power connections, opening up new avenues of innovation in consumer electronics, medical implants, and the deployment of sensor networks. However, inductive and Magnetic Coupled Resonance (MCR) approaches, known for safely delivering large amounts of power, are limited to relatively short transfer distances [1], [2]. As a result, these technologies are limited to charging electronic devices, such as electric toothbrushes and mobile phones at near contact distances [3]. In contrast, far-field wireless power transfer systems offer much longer ranges on the order of a few meters to kilometers but suffer from low transfer efficiency and low power levels due to safety concerns [4], [5]. Thus, far-field WPT solutions are typically limited to ultra-low-power applications such as UHF RFID tags [6], [7] and energy harvesting sensor nodes [8]–[10].

Previous work introducing Quasi-Static Cavity Resonance (QSCR), demonstrates the feasibility of generating near-field standing magnetic fields in the interior of a large room capable of safely delivering 10 s to 100 s of Watts of power to devices placed nearly anywhere within the room while complying with international safety guidelines (Fig. 1(a) [11], [12]. Although this approach shows unique strengths in safely delivering high-power levels to large volumes of space, the previous work on QSCR only provides analysis using coupled-mode theory (CMT) and finite element method (FEM)-based electromagnetic solvers, leaving a comprehensive circuit model unexplored [11]–[14]. Such CMT-based analysis does not provide sufficient insight into the system parameters that govern system performance and lacks utility when building peripheral systems. As seen in the progression of Magnetic Coupled Resonance WPT research, the transition from a CMT model to a circuit theory-based model for QSCR structures will allow

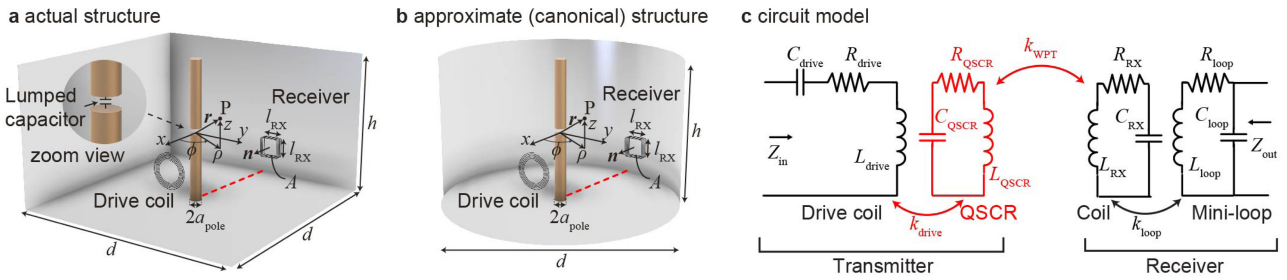

FIGURE 1. Overview of a QSCR-based WPT system. (a) Geometric setup of the QSCR developed in [11]. A square coil receiver and spiral drive coil is depicted within the QSCR. The coordinate systems shown here is used throughout the study. (b) A canonical, cylindrical shaped QSCR used for analysing the closed-form circuit model. (c) The circuit model of a QSCR-based WPT system, which is inspired by WPT systems using magnetically coupled resonators [15]. The circuit parameters we aim to compute is highlighted with red text.

comprehensive and intuitive system analysis; importantly, this transition offers a bridge to the wider electrical engineering community, enabling the development of new QSCR structures, transmitters and receivers, and applications [15], [16].

However, thus far, no closed-form solution of QSCR-based WPT systems that predict the magnetic field distribution and end-to-end power transfer efficiency exists. This is primarily due to the complicated current distribution on the structure's surfaces, making analysis approaches typically used in inductive and MCR-based WPT systems, such as Neumann's formula, inapplicable [17]. Furthermore, approaches for predicting the field and circuit model of conventional cavity resonators can not be used because the underpinning physics are different [18], [19]. Thus we need an effective circuit model that can accommodate variations in QSCR room geometry as well as receiver size, orientation, and position.

To address this need, this work explores circuit model analyses of QSCR-based WPT systems by formulating a closed-form circuit model of cylindrical QSCRs (Fig. 1(b), which, as explained in later sections, can be understood as a canonical form of the rectangular QSCR demonstrated in previous work [11], [18]. This cylindrical structure's symmetry allows formulating a closed-form circuit model (Fig. 1(c), and we experimentally show that we can use them to analyze rectangular QSCRs [11], [12]. We demonstrate the utility of this verified circuit model through designing impedance matching circuits that obtain high efficiency throughout a large volume, unraveling the factors dominating the performance of QSCR-based WPT systems, and optimizing the QSCR geometry.

II. OVERVIEW OF QUASI-STATIC CAVITY RESONATORS

Similar to traditional microwave cavity resonators [20], [21], Quasi-Static Cavity Resonators are hollow conductive structures that contain electromagnetic fields that oscillate in modal patterns. While the resonant frequency and field patterns of traditional microwave cavity resonators are defined by their geometry, Quasi-Static Cavity Resonators are specially designed to operate in the deep sub-wavelength region where the spatial length of the room is much smaller than the free space wavelength of the resonant frequency. This allows the system to effectively separate the magnetic fields that fills the interior of the structure (used for wireless power transfer) from the

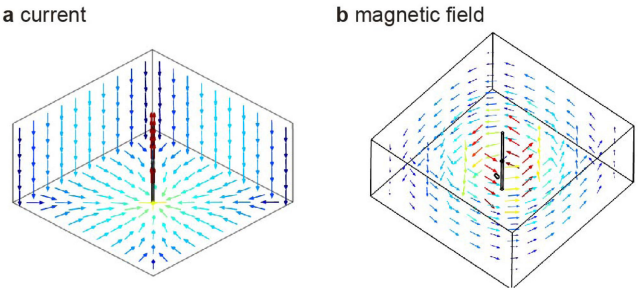

FIGURE 2. The current and the magnetic field distributions of a room-scale QSCR (4.9 m × 4.9 m × 2.3 m). (a) Surface currents (log scaled) flowing along the central pole, and around the exterior of the QSCR. They are colored by the log of the magnitude of the surface current (Red, large; Blue, small). (b) Log scaled Magnetic flux density vectors, colored by magnitude of magnetic flux density (Red, large; Blue, small).

potentially harmful electric fields that are stored in discrete lumped capacitors.

One of the observations from [11] is that the current induced on the walls, floors, and ceilings of the QSCR structure are proportional to the magnetic field pattern in the room and that by controlling the current flow, it is possible to control the magnetic field pattern and tune the resonant frequency of the structure. This is similar to how inductive coils and magnetically coupled resonators can be tuned by adding a capacitor to the coil. The conductive portions of the room behave as an inductor and form an *LC* resonator with lumped capacitors inserted within the central pole.

Fig. 1(a) shows the primary form of the QSCR structure consisting of a rectangular metallic enclosure, a metallic pole in the middle of the structure, and lumped capacitors inserted within the pole. When properly stimulated, current flows through the pole-ceiling-wall-floor-pole loop resulting in a large 3-D magnetic field pattern that permeates the interior of the space as shown in Fig. 2 which shows the current and magnetic fields distributions. This magnetic field enables the safe delivery of large amounts of power to receivers placed throughout the room [11], [12], [14]. A simulation-based safety evaluation of QSCR-based WPT incorporating an anatomical human body model showed that hundreds of Watts could potentially be delivered while complying with

international safety guidelines based on specific absorption rate (SAR) [11].

Previous work investigated QSCR using Coupled Mode Theory (CMT), revealing the fundamental physics underpinning this technology. However, the absence of a QSCR circuit model linked with geometric properties hinders the use of engineering tools such as circuit simulation and numerical optimization into QSCR-based WPT systems. We begin our analysis by overcoming the technical barrier in formulating circuit parameters of QSCR (*e.g.*, coupling coefficient) using geometrical properties and the receiver position as variables.

III. CIRCUIT MODEL ANALYSIS

This section aims to obtain a closed-form expression of the circuit model of QSCR, using the structure's geometry and the receiver's position as input. To this end, we suggest a simple circuit model as shown in Fig. 1(c), inspired by wireless power transfer systems using magnetically coupled resonators [15]. This model consists of a drive coil for coupling power to the room, the QSCR itself, and finally, a receiver with a resonant coil and a "mini-loop." This receiver topology using the "mini-loop" for impedance matching is common in wireless power transfer systems [22]. The drive coil is coupled to the QSCR via a mutually coupled inductors model, with a coupling coefficient, k_{drive}. Similarly, on the receiver side, the receiver is coupled to the cavity with a coupling coefficient, k_{WPT}. Thus, we can now view the entire operation of the QSCR as a simple repeater coil-type model that is common in wireless power transfer systems [23]–[25]. Among these parameters, we can analyze the inductance and resistance of the drive coil and the receiver, as is commonly found in the literature [17], [26], [27]. Thus, our analysis focuses on deriving the QSCR related parameters, highlighted in red in Fig. 1(c).

As a basic strategy, we compute L_{QSCR}, the inductance looking into the central pole's gap, and k_{drive}, k_{WPT}, the coupling between the QSCR and the coils, via the magnetic field distribution of QSCR. By definition, L_{QSCR} can be computed via the volume integral of the total magnetic field. k_{drive} and k_{WPT} can be retrieved via the surface integral of magnetic flux penetrating the coil's cross-section and the total magnetic energy confined in the volume by revisiting coupled-mode theory. Then, C_{QSCR}, defined by lumped capacitors, is determined by series resonant conditions, and R_{QSCR}, the ohmic loss of the QSCR, will be determined using the resistivity and the geometry of the current path. The remaining part of this section performs the calculation of these factors, incorporating the geometrical properties of the structure.

A. APPROXIMATE GEOMETRY USING A CYLINDRICAL CAVITY

Although the quasi-static cavity resonators built and analyzed in this work are rectangular in geometry, the mathematics greatly simplify for cylindrical type resonators, and it has been shown in previous work that cylindrical cavities have similar field distributions with rectangular ones [18]. Thus, we will first derive expressions for a cylindrical quasi-static cavity (see Fig. 1(b) and experimentally show that this expression well represents the characteristics of the square QSCR structure.

The currents flowing in/out of the floor and ceiling composed of perfect electric conductors can be modeled by a continuation of the current flowing in z-direction, as in classical image theory. Thus, the current flowing through the pole can be assumed to be infinitely long in the z-direction, and furthermore, we can approximate the field to be independent of the z-axis coordinate. In the rectangular case, the image is also caused by the walls, and the magnetic field can be expressed as the following [11]:

$$\mathbf{H}_{\text{rectangular}} = \frac{1}{2\pi}\sum_{m=-1}^{1}\sum_{n=-1}^{1}\frac{-I_0(-1)^{n+m}(y-md)}{(x-nd)^2+(y-md)^2}\mathbf{a_x} + \frac{I_0(-1)^{n+m}(x-nd)}{(x-nd)^2+(y-md)^2}\mathbf{a_y} \tag{1}$$

$\mathbf{a_x}$ and $\mathbf{a_y}$ are unit vectors of the rectangular coordinate. For cylindrical structures, the wall images can be ignored [28]; thus, the magnetic field of a cylindrical QSCR can be expressed as follows, using cylindrical coordinates:

$$\mathbf{H}_{\text{cylindrical}} = H_\phi \mathbf{a}_\phi = \frac{I_0}{2\pi}\frac{1}{\rho}\mathbf{a}_\phi \tag{2}$$

Here $\mathbf{a}_\phi$ is a unit vector of the cylindrical coordinates corresponding to ϕ in Fig. 1(a) and (b). Equation (2) corresponds to the $(m, n) = (0, 0)$, which is the dominant component of (1). Thus, cylindrical QSCR can be understood as a structure extracting the canonical elements of the rectangular QSCR, which justifies this approximation using cylindrical geometry.

In the following, we consider a cylindrical cavity with height, h, diameter, d, and central pole radius, a_{pole}. Referring to the implementation in [11], it is assumed that the central pole and the walls are composed of different materials, having conductivity σ_{pole} and σ_{wall}.

B. DERIVING INDUCTANCE AND CAPACITANCE

Using the magnetic field expression in (2), we can retrieve the cylindrical cavity's inductance looking into the pole's central gap from the magnetic energy stored in the QSCR. In particular, since the magnetic energy, E_{m}, stored in an inductor is $E_{\text{m}} = 1/2\, LI_0^2$ (L is inductance, and I_0 is the current flowing in the inductor), we need only compute the magnetic energy stored in the cylindrical cavity with volume V. This energy can be computed by using:

$$E_{\text{m}} = \iiint_V \frac{\mu_0}{2}|\mathbf{H}|^2 \mathrm{d}V \tag{3}$$

Without loss of generality, I_0 can be assumed to be unity, and we can use the result of (3) in the equation for energy stored by an inductor to solve for L, the inductance of the cavity. For

the cylindrical QSCR, the result is the following by using (2):

$$L_{\text{QSCR}} \approx L_{\text{cylindrical}} = \frac{\mu_0 h}{2\pi} \ln \frac{d}{2a_{\text{pole}}} \tag{4}$$

Then, we can determine the needed capacitor values from the series resonant condition $2\pi f_0 = 1/\sqrt{LC}$, where C is capacitor value and f_0 is the resonant frequency. This results in the following expression:

$$C_{\text{QSCR}} \approx C_{\text{cylindrical}} = \frac{1}{(2\pi f_0)^2 L_{\text{cylindrical}}}, \tag{5}$$

which can be implemented using lumped capacitors. In theory, the sum of the capacitance introduced by lumped elements and the parasitic capacitance of the cavity structure needs to match this capacitance for tuning the resonant frequency to f_0. However, because the parasitic capacitance is much smaller than C_{QSCR}, when using the geometry introduced in Fig. 1, the parasitic capacitance is omitted.

C. DERIVING RESISTANCE

Next, the focus shifts to determining the resistance of the QSCR. This resistance is essential because it sets the inductor's quality factor and significantly impacts the efficiency at which the cavity can transfer power to receivers contained within. When using the "skin effect" to compute the resistance it is assumed that the currents uniformly distribute across one skin depth of the metal (δ_{pole}, δ_{wall}), calculated using the conductivity and the given frequency.

Standard analysis for computing the resistance by integrating an assumed current density over the current path of the QSCR then leads to an expression for the resistance looking into the pole's central gap:

$$R_{\text{QSCR}} \approx R_{\text{cylindrical}} = \frac{h}{2\pi\sigma_{\text{wall}}\delta_{\text{wall}}}\left(\frac{2}{h}\ln\frac{d}{2a_{\text{pole}}} + \frac{2}{d}\right) + \frac{h}{2\pi\sigma_{\text{pole}}\delta_{\text{pole}}}\cdot\frac{1}{a_{\text{pole}}} \tag{6}$$

Furthermore, given the capacitance C_{QSCR} and quality factor Q_{C} of the lumped capacitor, the additional resistance by the capacitor can be calculated by $R_{\text{C}} = 1/(2\pi f_0 C_{\text{QSCR}} Q_{\text{C}})$. Although loss R_{C} will be added to (6) in reality, we will proceed with this analysis without accounting for this loss to investigate how the geometrical features affect the circuit parameters of the QSCR.

Next, because the Quality factor of an inductor is defined as $Q = 2\pi fL/R$, we can combine use (4) and (6) to get the quality (Q) factor of the cylindrical QSCR. For illustrating the general relationship between the geometry and Q-factor, the following shows the Q-factor assuming that the pole and the wall are made of the same material with conductivity σ:

$$Q_{\text{QSCR}} \approx Q_{\text{cylindrical}} = \frac{\frac{2}{\delta}hda_{\text{pole}}\ln\frac{d}{2a_{\text{pole}}}}{2da_{\text{pole}}\ln\frac{d}{2a_{\text{pole}}} + 2ha_{\text{pole}} + hd} \tag{7}$$

This expression will be used in Section V-D for optimizing the pole radius for maximizing the Q-factor of the cavity.

D. DERIVING COUPLING COEFFICIENT

This section first revisits coupled-mode theory to describe how the coupling coefficient can be calculated via the magnetic field distributions. Then, the derived abstract expression of the coupling coefficient is linked with the geometric properties of the structure to obtain a closed-form expression given input of the QSCR and receiver geometry and the receiver position.

In the following, we conduct analysis and experiments for deriving k_{WPT}, the coupling between the QSCR and receiver coil, because this significantly impacts efficiency [11]. Note that k_{drive}, the coupling coefficient between the QSCR and the drive coil, can be computed via the same procedure because the following analysis considers the coupling between the QSCR and general coil resonators.

1) COUPLED MODE THEORY

In previous work, we showed how coupling rate can be predicted using coupled mode theory [11], [20], [29]. In this case, the coupling rate, κ (rad/s) between the QSCR and coil receivers (rectangular or circular shape) can be found from the following [11], [20]:

$$\kappa = \frac{\sqrt{2}}{4}\frac{\omega_0\beta}{\sqrt{L_2\alpha}} \tag{8}$$

$$\alpha = \iiint_V \frac{\mu_0}{2}|\mathbf{H}|^2\,\mathrm{d}V \tag{9}$$

$$\beta = \iint_A \mu_0\mathbf{H}\cdot\mathbf{n}\,\mathrm{d}A \tag{10}$$

In the above, α is the total magnetic energy stored in the room; similarly, β is the flux captured by a receiver. Additionally, V is the volume of the enclosed cavity, $\mathbf{n}$ is the normal unit vector of the receiver's surface, ω_0 is the resonant frequency of the QSCR, A is the area enclosed by the receiver, and L_2 is the receiver's inductance. Generally speaking, V is the entire volume where the resonator generates electromagnetic fields, but the cavity volume can be used herein because high conductivity cavities confine the field to the interior.

Evaluation of these equations and substitution into (8) produces the coupling rate between the quasi-static cavity resonator and a receiver with one or more turns.

2) COUPLING COEFFICIENT

This coupling rate κ derived above is directly related to the coupling coefficients k in the circuit model. The relationship that transforms κ to k is given by the following [30]:

$$k = 2\kappa/\omega_0 \tag{11}$$

Note that coupling rate κ typically increases with frequency; thus, the coupling coefficient k is effectively frequency independent over the frequency ranges investigated in this work.

A method for analytically predicting κ was presented in Section III-D1, however, using the full expressions for the

fields formulated by (1) for computation of (8–10) is cumbersome and non-intuitive. Thus, the following analysis derives a simple expression that can be quickly evaluated for use in the circuit model. To do this, we consider the magnetic fields of a cylindrical cavity and assume a square-shaped receiver with multiple turns and a unit normal vector $\mathbf{n} = \mathbf{a}_\phi$ for simplicity. We note that the following analysis can be easily extended to other shaped receivers such as circles and rectangles. The analysis now proceeds with the necessary mathematics to get a simple approximation to the coupling rate and, subsequently, the coupling coefficient for a cylindrical cavity.

First, note that we are evaluating (8), and to do so we need α and β of (9) and (10). The current flowing through the pole I_0 is assumed to be unity; this assumption can be made without loss of generality. Then, from the definition of inductance, α becomes just 1/2 of the cylindrical cavity's inductance. This only leaves computation of β, which can be found by integrating (2) over the surface of a square-shaped receiver whose side length is l_{RX} with N_{RX} turns (the mathematics are simplified when using square coils).

Substituting the result into (8) and (11) the result is:

$$k_{\mathrm{WPT}} \approx k_{\mathrm{cylindrical}} = \frac{2\kappa}{\omega_0} = \frac{\mu_0 N_{\mathrm{RX}} l_{\mathrm{RX}}}{2\pi\sqrt{L_{\mathrm{RX}} L_{\mathrm{cylindrical}}}} \ln\left(\frac{\rho + l_{\mathrm{RX}}/2}{\rho - l_{\mathrm{RX}}/2}\right) \tag{12}$$

Thus, we have an easily evaluated approximation to the coupling coefficient for cylindrical cavities.

E. DERIVING THE EFFICIENCY

Once the circuit model is computed, the upper bound on efficiency, which we refer to as G_{max}, can be predicted assuming a perfectly lossless bi-conjugate impedance match [31], [32]. There are three necessary parameters for computing G_{max}, and these are: coupling rate κ, the Q-factor of the QSCR (Q_1), and Q-factor of the receiver (Q_2). Here, the Q-factor can be calculated via the expression for inductors: $Q = \omega L/R$. At the resonant frequency, ω_0, the expression for G_{max} using these parameters is

$$G_{\mathrm{max}} = \frac{\chi}{\left(1 + \sqrt{1+\chi}\right)^2} \tag{13}$$

$$\chi = \frac{4Q_1 Q_2 |\kappa|^2}{\omega_0^2}. \tag{14}$$

Using this expression combined with the developed circuit model, we can predict the upper bound on efficiency of a QSCR system based only on the system geometry.

IV. EXPERIMENTAL RESULTS

In this section, we will experimentally verify the theory described in the last section. We conducted measurements using a square, room-sized QSCR with dimensions of 4.9 m × 4.9 m × 2.3 m [11]. The floor, ceiling, and walls are made of painted aluminum (1100 alloy, 0.04" thick Al) sheet metal bolted to an aluminum frame (with grey carpet covering the floor). Fig. 3 shows a photograph of this system.

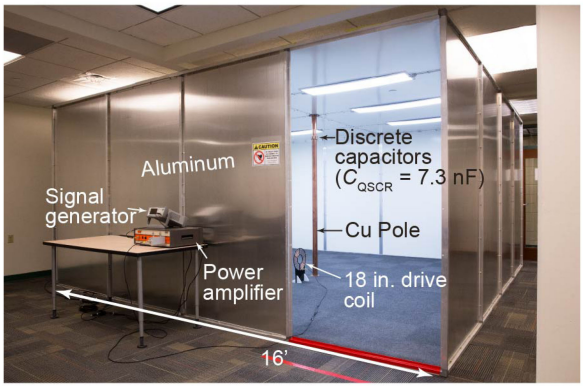

FIGURE 3. The room-sized, experimental QSCR used in this work. A tone matching the room's resonant frequency is input via a drive coil coupled to the room's magnetic field. Then, the room generates a 3-D magnetic field within the volume, and receivers within the system's coverage get powered.

The QSCR has a central copper pole with a diameter of 7.2 cm, with 15 high-Q, high voltage, discrete capacitors totaling 7.3 nF inserted across a 2.5 cm gap in the pole, producing resonance at 1.32 MHz. This operating frequency was chosen as it is the most permissive in terms of FCC field strength limits while still operating in the MHz region. It should be noted that QSCR-based wireless power transfer systems can easily operate at other frequencies based on the requirements of the end application. In this work we used a 6-turn, square coil receiver with a 16.5 cm side length made using 2 mm diameter copper wire. Finally, we used a 28 cm, 8-turn spiral drive coil for stimulating the room (Fig. 3). The quality factors of the QSCR and receiver are 2150 and 350, respectively, as measured using common RF techniques [33].

A. VERIFICATION OF THE CIRCUIT TOPOLOGY

The validity of using the circuit model assumed in Fig. 1(c), inspired by general magnetically coupled resonators, is inspected herein. To do this, we measure the Z-parameters of the three sub-circuits of Fig. 1(c) and then use a curve fitting routine to extract the circuit parameters from the measured Z-parameters. The source, source-coupled-to-QSCR, and receiver circuit are all measured individually by connecting a vector network analyzer (VNA) to the ports indicated as Z_{11} and Z_{22} in Fig. 4. Then we extracted the impedances of each component via fitting these Z_{11} and Z_{22} curves. This analysis is a standard method for deriving the circuit parameters of a wireless power transfer system [15], [34], [35]. A good match between the extracted and measured frequency-impedance curve will confirm the validity for using the circuit model in Fig. 1(c).

The results of the analysis are summarized in Fig. 4(a)–(c) as well as Table 2. Fig. 4 shows the analytic, extracted Z-parameters as well as the measured Z-parameters for the three

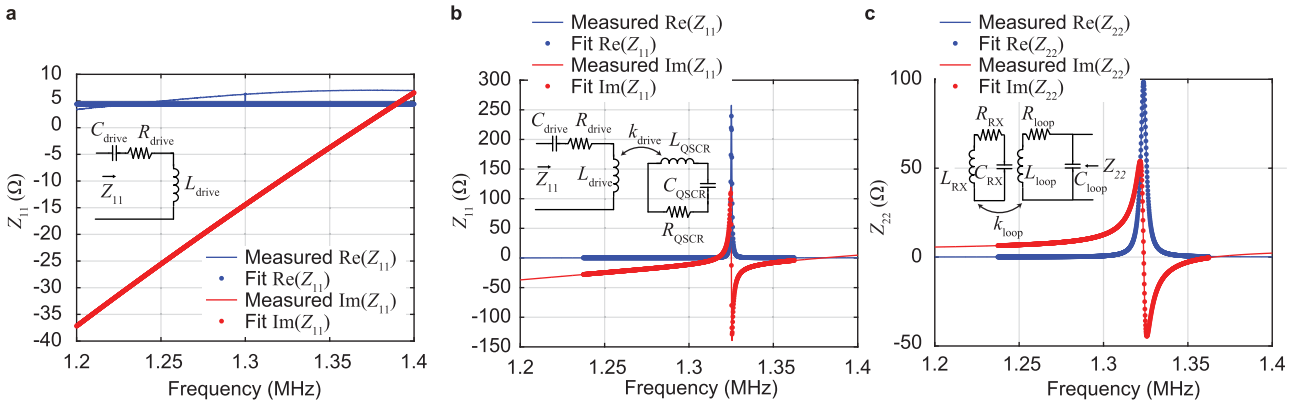

FIGURE 4. **Measured and extracted curves for the Z-parameters of the QSCR-based wireless power transfer system. The extracted curve is computed via three separate steps; each step takes measured data of a different part of the entire QSCR circuit: (a) is for the drive coil only, (b) is for the drive coil coupled to the QSCR, and (c) is for the receiver (with mini-loop) resonator. By assuring that the circuit model Z-parameters (Z_{11} and Z_{22}) match the measured Z-parameters, we have thus ensured that the circuit model and the element parameters are a good representation of the system.**

TABLE 1. **Extracted Circuit Parameters of the Rectangular QSCR**

Parameter	Value
R_{drive}	0.22 Ω
L_{drive}	16.4 µH
C_{drive}	822 pF
R_{QSCR}	10.1 mΩ
L_{QSCR}	2.02 µH
C_{QSCR}	7.14 nF
k_{drive}	0.031
R_{RX}	0.32 Ω
L_{RX}	12.66 µH
C_{RX}	1.14 nF
R_{loop}	15.4 mΩ
L_{loop}	573 nH
C_{loop}	556 pF
k_{loop}	0.244
r^2 coefficient	0.99

TABLE 2. **Analytic Circuit Parameters of the Cylindrical QSCR**

Parameter	Value	Analytic expression
$L_{\text{cylindrical}}$ ($\approx L_{\text{QSCR}}$)	1.94 µH	Eq. (4)
$C_{\text{cylindrical}}$ ($\approx C_{\text{QSCR}}$)	7.49 nF	Eq. (5)
$R_{\text{cylindrical}}$ ($\approx R_{\text{QSCR}}$)	4.5 mΩ	Eq. (6)
$k_{\text{cylindrical}}$ ($\approx k_{\text{WPT}}$)	variable	Eq. (12)

sub-circuits of the proposed circuit model. The correlation coefficient is greater than 0.99 in all cases, indicating a good match with the measured data model. Table 2, then provides the circuit parameter values of our experimental system extracted from this fitting routine.

B. VERIFICATION OF THE INDUCTANCE, CAPACITANCE, AND RESISTANCE MODEL

Next, the analytical expressions of inductance, capacitance, and resistance, derived as (4), (5), and (6), are verified by comparing them with the extracted results presented in Section IV-A. Table 2 shows these values calculated using the dimensions of $d = 4.9$ m, $h = 2.3$ m, and $a_{\text{pole}} = 0.036$ m. We assumed A1100 aluminum alloy for the wall/floor/ceiling material and copper as the pole material. Comparing with Table 2, which shows the results extracted from measurements, the inductance and capacitance well match the extracted results of the rectangular cavity.

The measured resistance, which was extracted via the fitting process, is higher than the analytic expressions. This additional few mΩ loss can be explained by the non-ideal construction techniques of the QSCR structure and the capacitors' Equivalent Series Resistance (ESR). For instance, the connections between different parts of the QSCR structure were made by bolting (*i.e.*, pressing) parts to each other instead of soldering for ease of construction. Furthermore, even if the capacitor has a Q-factor as high as $Q_{\text{C}} = 5000$, the additional ESR of the capacitor will be 3.2 mΩ, which is close to the error in the estimated resistance. Thus the most accurate estimation for resistance of the QSCR is typically obtained by direct measurement after construction. Nonetheless, (6) can be used to estimate the order of magnitude loss expected for an ideally built QSCR.

C. VERIFICATION OF THE COUPLING RATE MODEL

The expression of the coupling coefficient developed in Section III-D is experimentally validated herein. We measured the coupling coefficient by tuning the square receiver to the resonant frequency of the QSCR and then moving it around the interior of the QSCR (while keeping its unit normal vector $\mathbf{n} = \mathbf{a}_\phi$) and measuring the frequencies of the resulting hybrid modes. We used a VNA to record the S_{11} and recovered the coupling using previously developed techniques [1], [29], [36].

Fig. 5 shows the approximate expression (12) together with measured results, and these results are in good agreement. However, an error can be observed near the corner of the structure ($\phi \approx 45^\circ$, $\rho \approx d/2$). This error can be explained by the mirror image of the central pole current created by the walls. Near the corners, the analytic expression overestimates the wall image because the cylindrical QSCR's walls are closer than those of the rectangular QSCR. This observation well

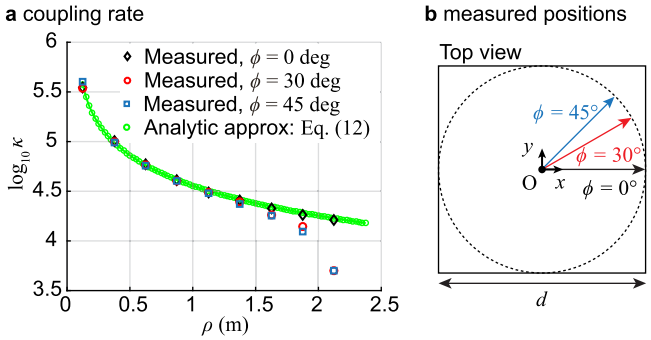

FIGURE 5. Measured and analytic results for the coupling rate along the line between the central pole and the edges of the room-scale QSCR. (a) Coupling coefficient as a function of the distance from the room center ρ. See (b) for the measured positions corresponding to each angle ϕ.

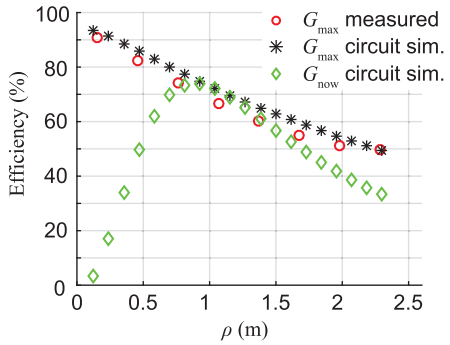

FIGURE 6. Measured and simulated relationship between power transfer efficiency and the distance from QSCR's center pole. G_{max} refers to the upper bound of efficiency, as described in Section III-E. G_{now} refers to the efficiency using static impedance matching circuits, as described in Section V-A.

matches the trend seen in Fig. 5, which shows that (12) results in a larger coupling than the measured value near the corners.

D. VERIFICATION OF THE POWER TRANSFER EFFICIENCY

Once the circuit parameters of QSCR is calculated, an upper bound on efficiency, which we refer to as $G_{\max}$, can be predicted assuming a perfectly lossless bi-conjugate impedance match [11], [31]. To calculate $G_{\max}$ from the circuit model, we ran circuit simulations in Keysight Advanced Design System (ADS), using the extracted circuit model parameters in Table II. Additionally, (12) was used to model the coupling between the receiver and the QSCR while moving the receiver from 0.125 m to 2.25 m away from the pole (along the red dotted line in Fig. 1(a). Then, the analytic efficiency was calculated from this coupling rate, (13), and (14). The results are plotted in Fig. 6 with the measured $G_{\max}$, which was calculated from the measured S-parameters [31]. The plots show that all the results are in good agreement, even though we use the approximate expression of coupling coefficient.

V. DISCUSSION

The formulation of inductance (4) and capacitance (5) of QSCRs implies that QSCRs can be built in various sizes, and the operating frequency can be tuned to the desired value independent of the system dimension. This feature makes this technology potentially applicable to various enclosures such as toolboxes, rooms, and factories as long as the space can introduce QSCR structures and the charging target devices can equip coil receivers. Meanwhile, the formulation of coupling (12) and efficiency (13) reveals how the power transfer efficiency will degrade as the size of the QSCR and the receiver deviates, allowing the estimation of the needed receiver size when a specific power level is required. In the rest of this section, we demonstrate the utility of the developed circuit model through several use cases and show that the presented circuit model can support assessing the applicability of this technology based on system geometry.

A. OPTIMIZING A STATIC IMPEDANCE MATCHING CIRCUIT

Given the circuit model, other well-known impedance matching and receiver design techniques have become available in the simulation environment to refine the QSCR's operation further. In this spirit, we used the same simulator as in Section IV-D to maximize the average efficiency along the red dotted line in Fig. 1(a) when using a static impedance matching circuit. G_{now} in Fig. 6 shows the efficiency along the line using a static impedance match (that is, the efficiency when the drive coil position and the receiver's "mini-loop" for impedance matching is static) optimized via this approach. Although efficiency will only be maximized at one distance away from the pole, the advantage here is that the impedance matching circuit remains static, without any re-tuning required.

B. DETERMINING THE QSCR AND RECEIVER SIZE

Design requirements for achieving a given efficiency across the room can now be formulated because the QSCR system's circuit model as a function of geometry is derived. Here, we show a case study for formulating the QSCR design conditions in which the efficiency exceeds 50% in most of the volume when the receiver is given. Note that this discussion can easily be extended to other efficiency values and the situation where the QSCR is given, and the receiver needs to be designed.

From (13), the condition for exceeding 50% efficiency is

$$\chi = \frac{4Q_1Q_2|\kappa|^2}{\omega_0^2} > 8. \tag{15}$$

The efficiency is typically high near the central pole and falls as the receiver approaches the walls. Thus, to analyse the lower end of efficiency, interest shifts to the situation where the receiver is close to the walls ($\rho \approx d/2$). In such conditions, $\rho \approx d/2 \gg l_{\text{RX}}$ holds, assuming that the receiver is much smaller compared to the room (which is true in most cases). Then, (12) can be approximated as the following:

$$\kappa \approx \frac{\omega_0\mu_0 N_{\text{RX}}}{4\pi\sqrt{L_{\text{RX}}L_{\text{QSCR}}}} \frac{l_{\text{RX}}^2}{\rho} \tag{16}$$

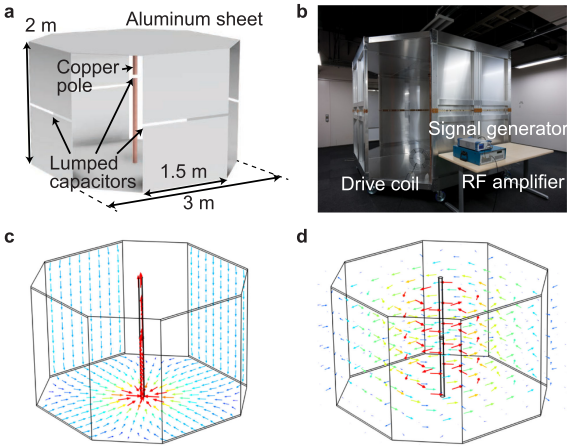

FIGURE 7. A QSCR-based system with openings in the corners of the room. Refer to [12] for the details on this design. (a) shows the structure of the resonator and (b) shows the experimental room-scale implementation. (c) and (d) show the simulated current and magnetic field distributions, which are identical to the implementation in Figs. 1 and 4.

The κ when the receiver reaches the wall (which is the low area of efficiency) can be calculated by using $\rho = d/2$ and by substituting (4),

$$\kappa \approx \frac{\omega_0 \mu_0 N_{\mathrm{RX}}}{4\pi \sqrt{L_{\mathrm{RX}} \frac{\mu_0 h}{2\pi} \ln \frac{d}{2a_{\mathrm{pole}}}}} \frac{2I_{\mathrm{RX}}^2}{d}. \tag{17}$$

By using (15), (17), and the Q-factor of an inductor, $Q = \omega L/R$, the condition for exceeding 50% efficiency in most of the volume can be expressed as the following:

$$\frac{d^2 h}{Q_{\mathrm{QSCR}}} \ln \frac{d}{2a_{\mathrm{pole}}} < \frac{\omega_0 \mu_0}{4\pi} \frac{N_{\mathrm{RX}}^2 I_{\mathrm{RX}}^4}{R_{\mathrm{RX}}} \tag{18}$$

The right side corresponds to receiver parameters; thus, if the QSCR features, corresponding to the left side of the formula, maintains this relationship, power efficiency will exceed 50% in most of the volume.

C. VERIFICATION OF THE COUPLING RATE MODEL USING A QSCR WITH APERTURES IN THE CORNERS

The expression of coupling rate (12) is compared with measured values using a QSCR with the walls on the corners removed to investigate the formulation's applicability for such design variations [12]. Fig. 7(a) and (b) shows the resonator used for this investigation; each corner of the rectangular cavity is cut off to form an aperture. The dimensions of this room-scale wireless power transfer system were 3 m × 3 m × 2 m. Among the two available resonant modes of this resonator, the mode which generates a magnetic field pattern resembling the original QSCR ($Q \approx 1200$) was used [12]. Fig. 7(c) and (d) shows the current distributions and magnetic field distribution of this mode. The floor, ceiling, and walls were made of 1 mm thick, 1100 aluminum alloy sheet metal bolted to aluminum frames, and the copper pole's diameter was 6 cm [12]. A

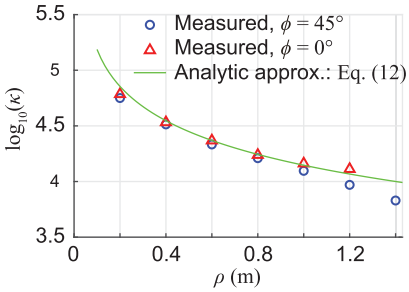

FIGURE 8. Measured and analytic coupling rate as a function of the distance from the room center ρ. Refer to Fig. 5(b) for the definition of angle ϕ.

6-turn, 100 mm square coil receiver, and a 300 mm, 6-turn spiral drive coil were used in the following measurements.

Fig. 8 shows the measured and the derived approximate coupling rate (12). These two curves well match around the center of the room, although the approximation is only strictly accurate for cylindrical cavities without apertures. As the receiver gets far from the pole, a small error discussed in Section IV-C occurs, strengthening the coupling on the $\phi = 0°$ receiver positions and weakening the coupling on the $\phi = 45°$ receiver positions.

D. OPTIMAL POLE RADIUS

Larger resonator width, d, and heights, h yield increasing Q-factors, owing to the fact that the resonator has a larger volume in which to store magnetic energy (and this increase in stored energy is larger than the increased ohmic losses that arise from adding more material). While the Q-factor is generally an increasing function of resonator diameter and height, a different result is seen for the pole's central radius, a_{pole}. For all other parameters fixed, we can find an optimal pole radius in terms of maximizing Q-factor by using the standard approach of differentiating (7) and setting equal to 0. This yields the following equation for the pole radius that maximizes the resonator's Q-factor.

$$a_{\mathrm{optimal}} = \frac{d}{2}\left(\ln \frac{d}{2a_{\mathrm{pole}}} - 1\right) \tag{19}$$

The above equation is a transcendental equation with no closed form solution. For a given d, it is possible to find a_{pole} such that the quality factor is optimized. However, a more generalized solution can be found by solving (19) for the *ratio* of a_{pole} to d. Doing this allows us to find the optimal pole radius to resonator diameter, valid for any cavity diameter. In this case, numerical solution of (19) for a_{pole}/d yields

$$a_{\mathrm{pole,optimal}}/d \approx 0.139. \tag{20}$$

Thus, if the objective is to maximize the cavity's quality factor, then the pole's radius should be approximately 14% of the cavity's diameter. This is not always possible in practical situations, but it still provides insight into what can be expected from an optimally constructed cavity.

VI. CONCLUSION

This paper explored the circuit model of QSCR-based wireless power transfer systems. We developed a closed-form expression for the coupling between the QSCR chamber and a receiver placed within by gaining intuition into the physical fields generated by these resonators, along with a circuit model and circuit parameters that govern the operation of such systems. The circuit model simplifies the description of this type of system's operation, offering a bridge with the foundation of circuit technology. These QSCR resonators permit power transfer on large scales but can also be scaled up or down to essentially any size. These wireless power systems offer a new paradigm in wireless power transmission that can provide a ubiquitous power delivery experience.

REFERENCES

[1] A. Kurs, A. Karalis, R. Moffatt, J. D. Joannopoulos, P. Fisher, and M. Soljačić, "Wireless power transfer via strongly coupled magnetic resonances," *Science*, vol. 317, no. 5834, pp. 83–86, 2007.

[2] S. Y. Hui, W. Zhong, and C. K. Lee, "A critical review of recent progress in mid-range wireless power transfer," *IEEE Trans. Power Electron.*, vol. 29, no. 9, pp. 4500–4511, Sep. 2014.

[3] J.-Q. Zhu, Y.-L. Ban, Y. Zhang, Z. Yan, R.-M. Xu, and C. C. Mi, "Three-coil wireless charging system for metal-cover smartphone applications," *IEEE Trans. Power Electron.*, vol. 35, no. 5, pp. 4847–4858, May 2020.

[4] J. Garnica, R. A. Chinga, and J. Lin, "Wireless power transmission: From far field to near field," *Proc. IEEE*, vol. 101, no. 6, pp. 1321–1331, Jun. 2013.

[5] N. Shinohara, "Power without wires," *IEEE Microw. Mag.*, vol. 12, no. 7, pp. S64–S73, Dec. 2011.

[6] S. A. Ahson and M. Ilyas, *RFID Handbook: Applications, Technology, Security, and Privacy*. Boca Raton, FL, USA: CRC Press, 2017.

[7] A. P. Sample, D. J. Yeager, P. S. Powledge, A. V. Mamishev, and J. R. Smith, "Design of an RFID-based battery-free programmable sensing platform," *IEEE Trans. Instrum. Meas.*, vol. 57, no. 11, pp. 2608–2615, Nov. 2008.

[8] A. P. Sample and J. R. Smith, "Experimental results with two wireless power transfer systems," in *Proc. IEEE Radio Wireless Symp.*, 2009, pp. 16–18.

[9] Powercast Corp., "P2110b module datasheet," Rev 3, 2016. Accessed: Sep. 1, 2021. [Online]. Available: https://www.powercastco.com/documentation/p2110b-module-datasheet/

[10] H. Jabbar, Y. S. Song, and T. T. Jeong, "RF energy harvesting system and circuits for charging of mobile devices," *IEEE Trans. Consum. Electron.*, vol. 56, no. 1, pp. 247–253, Feb. 2010.

[11] M. J. Chabalko, M. Shahmohammadi, and A. P. Sample, "Quasistatic cavity resonance for ubiquitous wireless power transfer," *PLoS One*, vol. 12, no. 2, pp. 1–14, 2017.

[12] T. Sasatani, A. P. Sample, and Y. Kawahara, "Room-scale magnetoquasistatic wireless power transfer using a cavity-based multimode resonator," *Nature Electron.*, vol. 4, no. 9, pp. 689–697, 2021.

[13] T. Sasatani, M. J. Chabalko, Y. Kawahara, and A. P. Sample, "Multimode quasistatic cavity resonators for wireless power transfer," *IEEE Antennas Wireless Propag. Lett.*, vol. 16, pp. 2746–2749, 2017.

[14] T. Sasatani, C. J. Yang, M. J. Chabalko, Y. Kawahara, and A. P. Sample, "Room-wide wireless charging and load-modulation communication via quasistatic cavity resonance," in *Proc. ACM Interactive, Mobile, Wearable Ubiquitous Technol.*, 2018, vol. 2, no. 4, pp. 1–23.

[15] A. P. Sample, D. A. Meyer, and J. R. Smith, "Analysis, experimental results, and range adaptation of magnetically coupled resonators for wireless power transfer," *IEEE Trans. Ind. Electron.*, vol. 58, no. 2, pp. 544–554, Feb. 2011.

[16] Y. Zhang, K. Chen, F. He, Z. Zhao, T. Lu, and L. Yuan, "Closed-form oriented modeling and analysis of wireless power transfer system with constant-voltage source and load," *IEEE Trans. Power Electron.*, vol. 31, no. 5, pp. 3472–3481, May 2016.

[17] T. Imura and Y. Hori, "Maximizing air gap and efficiency of magnetic resonant coupling for wireless power transfer using equivalent circuit and neumann formula," *IEEE Trans. Ind. Electron.*, vol. 58, no. 10, pp. 4746–4752, Oct. 2011.

[18] D. M. Pozar, *Microwave Engineering*. Hoboken, NJ, USA: Wiley, 2011.

[19] M. Shahmohammadi, M. J. Chabalko, and A. P. Sample, "Circuit model for resonant cavity mode enabled wireless power transfer," in *Proc. 46th Eur. Microw. Conf.*, 2016, pp. 747–750.

[20] M. J. Chabalko and A. P. Sample, "Resonant cavity mode enabled wireless power transfer," *Appl. Phys. Lett.*, vol. 105, no. 24, 2014, Art. no. 243902.

[21] I. Takano, D. Furusu, Y. Watanabe, and M. Tamura, "Cavity resonator wireless power transfer in an enclosed space with scatterers utilizing metal mesh," *IEICE Trans. Electron.*, vol. E100-C, no. 10, pp. 841–849, 2017.

[22] D. S. Ricketts, M. J. Chabalko, and A. Hillenius, "Experimental demonstration of the equivalence of inductive and strongly coupled magnetic resonance wireless power transfer," *Appl. Phys. Lett.*, vol. 102, no. 5, 2013, Art. no. 053904.

[23] D. Ahn and S. Hong, "A study on magnetic field repeater in wireless power transfer," *IEEE Trans. Ind. Electron.*, vol. 60, no. 1, pp. 360–371, Jan. 2013.

[24] J. Qu and C. K. Lee, "Dynamic modeling for the wireless power transfer system in domino structure," *IEEE Trans. Ind. Electron*., vol. 69, no. 4, pp. 3556–3565, Apr. 2022.

[25] J. Lee and K. Lee, "Effects of number of relays on achievable efficiency of magnetic resonant wireless power transfer," *IEEE Trans. Power Electron.*, vol. 35, no. 7, pp. 6697–6700, Jul. 2020.

[26] K. Fotopoulou and B. W. Flynn, "Wireless power transfer in loosely coupled links: Coil misalignment model," *IEEE Trans. Magn.*, vol. 47, no. 2, pp. 416–430, Feb. 2011.

[27] J. Kim and Y.-J. Park, "Approximate closed-form formula for calculating ohmic resistance in coils of parallel round wires with unequal pitches," *IEEE Trans. Ind. Electron.*, vol. 62, no. 6, pp. 3482–3489, Jun. 2015.

[28] K. Kaiser, *Electromagnetic Compatibility Handbook*. Boca Raton, FL, USA: CRC Press, 2004.

[29] M. J. Chabalko and A. P. Sample, "Three-dimensional charging via multimode resonant cavity enabled wireless power transfer," *IEEE Trans. Power Electron.*, vol. 30, no. 11, pp. 6163–6173, Nov. 2015.

[30] M. Chabalko, E. Alarcon, E. Bou, and D. S. Ricketts, "Optimization of WPT efficiency using a conjugate load in non-impedance matched systems," in *Proc. IEEE Antennas Propag. Soc. Int. Symp.*, 2014, pp. 645–646.

[31] M. Zargham and P. G. Gulak, "Maximum achievable efficiency in near-field coupled power-transfer systems," *IEEE Trans. Biomed. Circuits Syst.*, vol. 6, no. 3, pp. 228–245, Jun. 2012.

[32] Y. Narusue, Y. Kawahara, and T. Asami, "Maximizing the efficiency of wireless power transfer with a receiver-side switching voltage regulator," *Wireless Power Transfer*, vol. 4, no. 1, pp. 42–54, 2017.

[33] E. Bou, E. Alarcon, and J. Gutierrez, "A comparison of analytical models for resonant inductive coupling wireless power transfer," in *Proc. Prog. Electromagn. Res. Symp.*, 2012, pp. 689–693.

[34] D. Kajfez and E. J. Hwan, "Q-factor measurement with network analyzer," *IEEE Trans. Microw. Theory Techn.*, vol. 32, no. 7, pp. 666–670, Jul. 1984.

[35] M. Shahmohammadi, M. Chabalko, and A. P. Sample, "High-Q, over-coupled tuning for near-field RFID systems," in *Proc. IEEE Int. Conf. RFID*, 2016, pp. 1–8.

[36] A. Bodrov and S.-K. Sul, "Analysis of wireless power transfer by coupled mode theory (CMT) and practical considerations to increase power transfer efficiency," *Wireless Power Transfer - Principles and Engineering Explorations*. London, UK.: INTECH, 2012.